Journal of Natural and Artificial Systems, 2026, 4(2): 199-217

Path Integral Monte Carlo Study of Ground State Properties of the Lithium Atom

Okoi, Peter Obeten, Obu, Joseph Abebe, Inyang, Etido Patrick
Received: 12 June 2026/Accepted: 23 August 2026/Published: 29 September 2026

Abstract : *In this work, the path Integral Monte Carlo(PIMC) is employed to estimate the ground-state properties of the lithium atom. The three-electron system is formulated in atomic units and represented by discretized imaginary-time paths. The ($1s^2$ $2s^1$) electronic configuration is used to construct the antisymmetric trial state, while a Jastrow correlation function is employed to incorporate electron–electron correlations. The total ground-state energy and its kinetic and potential components are calculated together with selected structural and correlation properties. Systematic convergence is investigated with respect to inverse temperature, the number of Trotter slices, and Monte Carlo sampling, while statistical uncertainties are evaluated by considering autocorrelation and block averaging. The calculated results are subsequently compared with high-precision theoretical benchmarks and with established electronic-structure and quantum Monte Carlo methods. The study has established a theoretical and computational PIMC framework for accurate and reliable determination of the ground properties of lithium atom which can be extended to other correlated atomic systems.*

Keyword: *Path integral, Kernel, propagator, Schrodinger equation, action, Lagrangian, Monte Carlo, Metropolis-Hasting, wick's rotation, partition function.*

Peter Obeten Okoi,
Department of Physics,
Faculty of Physical Science, University of Calabar, Calabar, Nigeria
Email: okoipeter7@gmail.com
https://orcid.org/0000-0001-9147-425X

Joseph Abebe Obu,
Department of Physics, Faculty of Physical Science,
University of Calabar, Calabar, Nigeria
Email: abebeobu@yahoo.com
https://orcid.org/0000-0001-9633-4045

Etido Patrick Inyang
Department of Physics, Faculty of Science, National Open University of Nigeria, Jabi-Abuja, Nigeria
Email: etidophysics@gmail.com
https://orcid.org/0000-0002-5031-3297

1.0 Introduction

Accurately determining atomic ground-state properties remains a fundamental objective in quantum physics because it provides essential information about atomic stability, electron distribution, electron–electron interactions, and correlation effects. Although the nonrelativistic Schrödinger equation provides the theoretical foundation for describing atomic systems, obtaining accurate solutions for many-electron atoms is challenging because of the coupled motion of electrons, Coulomb repulsion, and the requirement that the total electronic wavefunction satisfy fermionic antisymmetry. Consequently, few-electron atoms have become important benchmark systems for evaluating the reliability of analytical, variational, and stochastic computational methods (King & Shoup, 1986; Sims & Hagstrom, 2009). The lithium atom is particularly suitable for this purpose because it contains three interacting electrons and exhibits important correlation effects despite its relatively simple electronic structure.

In its ground state, lithium has the electronic configuration ($1s^2$ $2s^1$), comprising two core electrons and one valence electron. The ground-state properties are determined by the

combined effects of electron–nucleus attraction, electron–electron repulsion, exchange, and electronic correlation. An accurate computational description must therefore reproduce not only the total ground-state energy but also the spatial distribution of electrons and their mutual correlations. King & Shoup (1986) investigated the lithium atom using accurate electronic-structure calculations, while Sims & Hagstrom (2009) employed a Hylleraas configuration-interaction approach to examine the ground state and several excited states. Similarly, Gálvez *et al*. (2000) calculated correlated one-electron and two-electron densities for the lithium ground state, demonstrating the importance of electronic correlation in describing atomic structure. These studies establish lithium as a useful reference system for testing computational approaches to correlated many-electron problems.

Conventional electronic-structure methods provide important foundations for such calculations. Hartree–Fock theory accounts for exchange through an antisymmetric single-determinant wavefunction but does not fully describe electron correlation. Configuration-interaction and explicitly correlated methods improve the wavefunction by incorporating contributions from multiple electronic configurations and interelectronic coordinates. The work of López Ríos *et al*. (2006) demonstrated the usefulness of correlated wavefunctions for describing atoms across a broad range of the periodic table. Nevertheless, achieving high accuracy in correlated electronic systems remains computationally demanding, motivating the continued development of alternative approaches capable of sampling complex many-body distributions efficiently.

Quantum Monte Carlo (QMC) methods address this challenge by combining quantum-mechanical formulations with stochastic sampling. Variational Monte Carlo estimates expectation values using a trial wavefunction, whereas diffusion Monte Carlo uses imaginary-time projection to suppress contributions from excited states and approach ground-state properties. These methods have been widely investigated for atoms, molecules, and condensed-matter systems because they can treat electron correlation more explicitly than simple mean-field approaches (Austin *et al*., 2012; Foulkes *et al*., 2001; Needs *et al*., 2010). However, their accuracy and computational efficiency depend on the quality of the trial wavefunction, the sampling strategy, and the treatment of fermionic antisymmetry.

Path Integral Monte Carlo (PIMC) offers a complementary framework for investigating quantum systems by expressing quantum-mechanical quantities as integrals over particle trajectories in imaginary time. The method originates from Feynman's path-integral formulation of quantum mechanics (Feynman, 1948) and can be connected to statistical-mechanical partition functions through imaginary-time evolution. Trotter's product formula provides a mathematical basis for discretizing the evolution operator into finite time slices (Trotter, 1959), while subsequent developments established path-integral methods as important tools for studying quantum statistical systems (Ceperley, 1995; Feynman & Hibbs, 1965). In PIMC, the quantum problem is transformed into a sampling problem over discretized paths, allowing relevant thermodynamic and structural quantities to be estimated statistically. Reviews by Ceperley (1995) and Westbroek *et al*. (2018) discuss the theoretical foundations and computational implementation of path-integral sampling.

The ground-state limit can be investigated by considering sufficiently low temperatures, corresponding to large inverse temperatures, and controlling the discretization error associated with the number of imaginary-time

slices. Under appropriate conditions, contributions from excited states become progressively suppressed, allowing ground-state properties to be estimated from the sampled quantum distribution. The accuracy of these estimates depends on convergence with respect to temperature and time-slice discretization, the efficiency of the sampling algorithm, and the treatment of electron exchange. Metropolis–Hastings sampling provides a general framework for generating configurations from a target distribution, building on the foundational Monte Carlo method of Metropolis *et al*. (1953) and the generalization introduced by Hastings (1970). Path-integral formulations and related computational techniques have subsequently been applied to quantum many-body systems, including light nuclei, quantum dots, and condensed matter (Chen & Schmidt, 2022; Dornheim, 2019; Pollet, 2012).

A major challenge in applying conventional PIMC to the lithium atom is the fermion sign problem. Because electrons are indistinguishable fermions, exchanging two electron coordinates changes the sign of the wavefunction. The resulting path contributions can therefore have positive or negative weights, producing cancellations that increase statistical uncertainty, particularly at low temperatures. Ceperley (1991, 1995) examined the role of fermionic nodes and the sign problem in quantum Monte Carlo, while later studies investigated sign-problem limitations and possible bounds or special cases in fermionic simulations (Chin, 2023; Zhang *et al*., 2022). Fixed-node and restricted-path approaches offer practical ways to constrain the sampling using an approximate nodal structure. However, the quality of that structure can introduce systematic errors, as discussed by Anderson (1995), Reynolds *et al*. (1982), and Rasch *et al*. (2012). These limitations make careful validation and transparent assessment of convergence essential when PIMC is used for correlated electronic systems.

Although extensive research has examined lithium using high-accuracy wavefunction methods and has developed PIMC and related QMC techniques for many-body systems, a focused computational assessment of the lithium ground state using the particular path-integral and Metropolis–Hastings framework adopted in this study remains valuable. In particular, the relationship between the estimated ground-state energy and complementary observables—including electron density and ionization energy—should be assessed alongside numerical convergence and consistency with established lithium calculations. A systematic comparison with correlated electronic-structure results can help determine whether the proposed implementation captures the essential physical features of the three-electron atom and identify limitations associated with its approximations.

The aim of this study is to investigate the ground-state properties of the lithium atom using a Path Integral Monte Carlo framework. Specifically, the study formulates the path-integral representation through imaginary-time transformation, relates the resulting statistical formulation to the quantum-mechanical Hamiltonian, and implements Monte Carlo sampling using the Metropolis–Hastings algorithm. It estimates the ground-state energy, ionization energy, and electron-density distribution and evaluates the consistency of the results with established theoretical studies. The significance of the work lies in assessing the usefulness of a stochastic path-integral approach for a fundamental correlated-electron system. By examining both energetic and structural observables, the study seeks to provide a basis for further development of computational methods applicable to more complex atoms and quantum many-body systems.

The remainder of the paper is organized as follows. Section 2 presents the theoretical foundation of the path-integral formulation, including imaginary-time transformation, the partition-function connection, and the estimator used for ground-state calculations. Section 3 describes the Monte Carlo sampling procedure and the Metropolis–Hastings algorithm. Section 4 presents and discusses the calculated ground-state properties and comparisons with available theoretical results. Section 5 summarizes the principal findings and conclusions.

2.0 Path integral formulation of quantum mechanics

2.1 Formulation and Trotter slicing

The time-dependent Schrödinger equation for a non-relativistic particle of mass m moving in a one-dimensional potential V (z) with the Hamiltonian expressed as the sum of the kinetic- and potential-energy operators, H=T+V_z, is given by (Feynman, 1948; Feynman & Hibbs, 1965; Trotter, 1959). is

$$i\hbar\frac{d}{dt}\psi(z,t) = \hat{H}\psi(z,t) \quad (1)$$

And the corresponding evolution operator is

$$\hat{U}(t,t') = e^{-\frac{i}{\hbar}(t-t')H} \quad (2)$$

So that $|\psi(t)\rangle = \hat{U}(t,t')|\psi(t')\rangle$. By introducing position eigen states, the solution of eq. (1) is,

$$\langle z|\psi(t)\rangle = \psi(z,t) = \int K(z,t;z',t')\psi(z',t')dz' \quad (3)$$

where $K(z,t;z',t') = \langle\langle z|\hat{U}(t,t')|z'\rangle = \langle\langle z|e^{-\frac{i}{\hbar}(t-t')H}|z'\rangle$ (4)

It is represented by the density matrix, also known as the propagator (Feynman & Hibbs, 1965). To obtain a real and positive statistical weight suitable for Monte Carlo sampling, A Wick rotation is performed to transform real time into imaginary time (Feynman & Hibbs, 1965; Ceperley, 1995; Dornheim, 2019)., $t = -i\tau$, where τ is imaginary time. So that $e^{-\frac{i}{\hbar}tH} \rightarrow e^{-\frac{1}{\hbar}\tau H}$. And the imaginary time propagator becomes

$$\lambda(z,z';\beta) = \langle\langle z|e^{-\beta H/\hbar}|z'\rangle \quad (5)$$

where $\beta = \hbar/k_B T$

The imaginary-time interval is divided into P slices as $\beta = P\Delta\tau$The Trotter decomposition can therefore be expressed as follows (Trotter, 1959; Suzuki, 1976).

$$e^{-\beta H/\hbar} = \lim_{P\to\infty}\left[e^{-\Delta\tau T/\hbar}e^{-\Delta\tau V/\hbar}\right]^P + O(\Delta\tau^2) \quad (6)$$

A higher-order factorization may subsequently be employed to reduce time-step discretization errors. By inserting \(P-1\) complete sets of position eigenstates into the propagator, the path-integral representation can be obtained (Feynman & Hibbs, 1965; Ceperley, 1995) as $I = \int dz_j|z_j\rangle\langle z_j|$ to give

$$\lambda(z_P,z_0;\beta) = \int dz_1 \ldots . dz_{P-1}\prod_{j=1}^{P}\langle z_j|e^{-\Delta\tau T/\hbar}e^{-\Delta\tau V/\hbar}|z_{j-1}\rangle \quad (7)$$

Where $z = z_P$

For a free particle, the propagator using the gaussian integral

$$\int e^{-az^2+bz}dz = \sqrt{\frac{\pi}{a}}e^{b^2/4a} \quad (8)$$

Eq. (7) is evaluated to obtain

$$\langle z_j|e^{-\Delta\tau T/\hbar}e^{-\Delta\tau V/\hbar}|z_{j-1}\rangle = \left(\frac{m}{2\pi\Delta\tau\hbar}\right)^{1/2} e^{\left(-\frac{m\left(z_j-z_{j-1}\right)^2}{2\Delta\tau\hbar}\right)} \quad (9)$$

$$\text{So, } \lambda(z_P, z_0; \beta) = \left(\frac{m}{2\pi\Delta\tau\hbar}\right)^{P/2} \int dz_1 \ldots . dz_{P-1} e^{S_E/\hbar} \quad (10)$$

where the discretized Euclidean action is

$$S_E = \sum_{j=1}^{P} \left[\frac{m\left(z_j-z_{j-1}\right)^2}{2\Delta\tau\hbar} + \Delta\tau V(z_j)\right] \quad (11)$$

In the continuum limit, as the number of time slices approaches infinity, the discretized path-integral formulation converges to its continuous representation (Feynman & Hibbs, 1965; Ceperley, 1995; Dornheim, 2019; Feynman, 1948).

$$S_E[z(\tau)] = \int_0^\beta \left[\frac{m}{2}\left(\frac{dz}{d\tau}\right)^2 + V(z)\right] d\tau \quad (12)$$

Consequently

$$\lambda(z_P, z_0; \beta) = \int Dz(\tau) e^{(S_E[z(\tau)])/\hbar} \quad (13)$$

2.2 Partition function

The canonical partition function is

$$Z(\beta) = Tr\left[e^{-\beta H/\hbar}\right] \quad (14)$$

And in position representation,

$$Z(\beta) = \int \langle z|e^{-\beta H/\hbar}|z'\rangle \quad (15)$$

$$\text{Hence, } Z(\beta) = \left(\frac{m}{2\pi\Delta\tau\hbar}\right)^{P/2} \int dz_1 \ldots . dz_{P-1} e^{S_E/\hbar} \quad (16)$$

The quantum particle has therefore been transformed into a classical-like ring polymer consisting of PP imaginary-time beads; $z_0, z_1 \ldots, z_{P-1}$ with bead P connected back to bead 0. Considering eq. (11), then, the configuration probability sampled by PIMC is

$$\pi(z) = \frac{e^{S_E/\hbar}}{Z(\beta)} \quad (17)$$

The energy expectation is obtained from the partition function as

$$E(\beta) = -\hbar \frac{\partial}{\partial\beta} \ln Z(\beta) \quad (18)$$

Using the spectral representation

$$Z(\beta) = \sum_{n=0}^{\infty} e^{-\beta E_n/\hbar} \quad (19)$$

$$\text{So, } E(\beta) = \frac{\sum_{n=0}^{\infty} E_n e^{-\beta E_n/\hbar}}{\sum_{n=0}^{\infty} e^{-\beta E_n/\hbar}} \quad (20)$$

As imaginary time increases ($\beta \to 0$), contributions from excited states are exponentially suppressed, leaving the ground state as the dominant contribution (Feynman & Hibbs, 1965; Feynman, 1948; Ceperley, 1991; Ceperley, 1995; Dornheim, 2019; Foulkes *et al*., 2001; Needs *et al*., 2010; Austin *et al*., 2012).

$$E_0 = \lim_{\beta\to 0} E(\beta) \quad (21)$$

This provides the connection between finite-temperature PIMC and ground-state quantum Monte Carlo

2.3 Fermionic sign problem and approximations

Electrons, however, are fermions; therefore, their many-body wavefunction must satisfy the antisymmetry principle under the exchange of any two electrons (Pauli, 1925; Ceperley, 1991).

$$\psi(\ldots, r_i, \ldots r_j, \ldots) = -\psi(\ldots, r_j, \ldots . r_i, \ldots) \quad (22)$$

Consequently, the fermionic density matrix is obtained by antisymmetrizing the distinguishable-particle density matrix with $R = (r_1, r_2, \ldots . r_N)$ and κ is permutation of particle labels

$$\lambda_F(R, R'; \beta) = \frac{1}{N!}\sum_{\kappa}(-1)^{\kappa}\lambda(R, \kappa R'; \beta) \quad (23)$$

Slater Jastrow

A practical way of imposing fermionic antisymmetry is to use a Slater determinant. For N electrons, the Slater determinant is given as

$$D(R) = \frac{1}{\sqrt{N!}}\det\left[\phi_i(r_j)\right]$$

For lithium, a simple spin-orbital representation is

$$D(R) = \frac{1}{\sqrt{3!}}\begin{vmatrix}\phi_1(r_1) & \phi_1(r_2) & \phi_1(r_3)\\ \phi_2(r_1) & \phi_2(r_2) & \phi_2(r_3)\\ \phi_3(r_1) & \phi_3(r_2) & \phi_3(r_3)\end{vmatrix} \quad (24)$$

The Slater determinant accounts primarily for antisymmetry, whereas the Jastrow factor incorporates electron correlation

$$J(R) = e^{U(R)} \quad (25)$$

where $U(R) = \sum_{i<j}\frac{ar_{ij}}{1+br_{ij}} + \sum_{i,A}\chi(r_i, A)$ (26)

So, the trial wavefunction is therefore written as (Toulouse and Umrigar, 2008; Umrigar *et al*., 2007)

$$\psi_T(\kappa R) = (-1)^{\kappa}\psi_T(R) \quad (27)$$

where $\psi_T(R) = D(R)J(R)$

Thus, antisymmetry comes from the Slater determinant while dynamical correlation is introduced through J(R)

i. Importance sampling

Direct PIMC samples

$$\pi(R) \propto e^{-S_E(R)/\hbar} \quad (28)$$

However, sampling can be improved by incorporating information from a trial wavefunction. Define the importance-sampled distribution

$$f(R, \tau) = \psi_T(R)\psi(R, \tau) \quad (29)$$

For a positive trial amplitude within a nodal pocket, the corresponding importance-sampled imaginary-time equation becomes

$$-\frac{\partial f}{\partial \tau} = -\frac{1}{2}\nabla^2 f + \nabla.[F(R)f] + [E_L(R) - E_T]f \quad (30)$$

in atomic units, where the drift force, (Foulkes *et al*., 2001; Austin *et al*., 2012) is

$$F(R) = \nabla \ln|\psi_T(R)| = \nabla ln|D(R)| + \nabla J(R) \quad (31)$$

and

$$E_L(R) = \frac{H\psi_T(R)}{\psi_T(R)} \quad (32)$$

Hence both the determinant and Jastrow factor contribute to the drift

ii. Fixed node

For fermions, unrestricted sampling encounters the sign problem because positive and negative contributions cancel. The fixed-node approximation addresses this by imposing

$$\psi(R, \tau) = 0, \text{ whenever } \psi_T(R) = 0 \quad (33)$$

Thus, the nodal surface of the exact fermionic wavefunction is approximated by the nodal surface of the trial wavefunction (Ceperley, 1991; Reynolds *et al*., 1982).

The fixed-node density matrix may be written schematically as

$$\lambda_{FN}(R,R';\beta) = \int_{R(0)=R}^{R(\beta)=R'} DR(\tau) e^{(S_E[R(\tau)])/\hbar} \ominus_{FN} [R(\tau)] \quad (34)$$

Where $\ominus_{FN}[R(\tau)] = \begin{cases} 1, & for\ R(\tau)\ inside\ the\ region \\ 0, & otherwise \end{cases}$ (35)

Thus, a proposed path that crosses the nodal surface is rejected.

For the Slater–Jastrow trial state, the nodes are determined by D(R)=0.

The Jastrow factor changes the amplitude but, for a positive Jastrow factor, does not change the nodal surface.

iii. PIMC probability distribution

For the P-slice representation, we define $R_j = (r_{1,j}, r_{2,j}, \ldots . r_{N,j})$ and the complete path configuration is $\mathcal{R} = (R_0, R_1, \ldots . R_{P-1})$, where $R_P = R_0$ for ordinary periodic paths, or the appropriate antisymmetric permutation boundary condition for fermions. The discretized Euclidean action becomes

$$S_E = \sum_{j=0}^{P-1} \left[\frac{m}{2\Delta\tau} \left| R_{j+1} - R_j \right|^2 + \Delta\tau V(R_j) \right] \quad (36)$$

The PIMC sampling distribution is therefore

$$\pi(R) \propto e^{-S_E(R)/\hbar} |\psi_T(R_0)|^2 \ominus_{FN} [\mathcal{R}] \quad (37)$$

iv. Estimators

The thermodynamic energy estimator follows from eq. (18), so for a d-dimensional system of N particles, the primitive thermodynamic estimator has the form

$$E = \frac{NdP}{2\beta} - \frac{mP}{2\beta^2\hbar^2} \sum_{j=0}^{P-1} \left| R_{j+1} - R_j \right|^2 + \frac{1}{P} \sum_{j=0}^{P-1} V(R_j) \quad (38)$$

This estimator can have large variance when P is large, and so, a virial estimator is often preferable

For a Hamiltonian, H=T+V, the quantum virial theorem for a bound stationary state gives

$$2\langle T \rangle = \langle \sum_i^{\square} r_i . \nabla_i V \rangle \quad (39)$$

Therefore, for an N-electron system (Chin, 2023; Toulouse and Umrigar, 2008; Austin *et al*., 2012; Umrigar *et al*., 2007)

$$E_0 = \langle T \rangle + \langle V \rangle = \langle V(R) + \frac{1}{2} \sum_i^{\square} r_i . \nabla_i V\ (R) \rangle \quad (40)$$

3.0 Method

3.1 Metropolis-Hasting algorithm

The Metropolis–Hastings algorithm follows a sequence of steps for generating samples from the target probability distribution (Metropolis *et al*., 1953; Hastings, 1970; Foulkes *et al*., 2001; Needs *et al*., 2010).

i. Generate an initial configuration $\mathcal{R} = (R_0, R_1, \ldots . R_{P-1})$ inside an allowed nodal pocket

ii. Evaluate $\psi_T(R)$ and $= \nabla \ln|\psi_T(R)|$

iii. Choose an imaginary-time slice j and propose a possible move $R_j' = R_j + F_j\Delta\tau + \sqrt{\Delta\tau\eta}$, where η is a normally distributed random vector

iv. If $\psi_T(R')\psi_T(R) < 0$ and the path crosses the prescribed nodal surface, reject the move

v. The metropolis ratio is $A = min\left[1, \frac{\pi(\mathcal{R}')}{\pi(\mathcal{R})}\right]$

vi. Generate random number $U[0,1]$. And accept the move if $U < A$, otherwise, retain the previous configuration

vii. After equilibration, calculate E, $\langle V \rangle$ and $\langle T \rangle$ and other observables from statistically independent or appropriately decorrelated configurations.

viii. Divide the Markov chain into blocks and calculate

$$\langle E \rangle = \frac{1}{M}\sum_{k=1}^{M} E_k \quad (41)$$

The standard error is estimated from the block variance

$$\sigma_{\langle E \rangle} = \sqrt{\frac{\sigma_E^2}{M}} \quad (42)$$

Block averaging is important because successive Monte Carlo configurations are correlated

3.2 Dimensionless units

In PIMC, it is advantageous to express the governing equations in dimensionless form**.** Dimensionless units simplify the mathematical formulation, improve numerical stability, reduce computational cost, and eliminate the need to repeatedly handle extremely large or small physical constants. For atomic systems such as the lithium atom, atomic units (a.u.) are commonly employed because they naturally match the characteristic scales of electrons and nuclei.

In the atomic unit system, four fundamental physical constants are defined to be unity; $\hbar = e = m_e = 4\pi\epsilon_0 = 1$, where $\hbar$ is the reduced Planck constant, e is the elementary charge, m_e is the electron mass ϵ_0 is the vacuum permittivity. With these definitions, many physical quantities become dimensionless. The unit of length is the Bohr radius $a_0 = 4\pi\epsilon_0\hbar^2/m_e e^2 = 0.529177\ A^{\circ}$, while the unit of energy is the Hartree energy $E_h = e^2/4\pi\epsilon_0 a_0 = 27.211386\ eV$ (Tiesinga *et al*., 2021).

The Hamiltonian lithium atom in dimensionless units is given as;

$$H = \frac{1}{2}(\nabla_1^2 - \nabla_2^2 - \nabla_3^2) - 3\left(\frac{1}{r_1} - \frac{1}{r_2} - \frac{1}{r_3}\right) + \left(\frac{1}{r_{12}} + \frac{1}{r_{13}} + \frac{1}{r_{23}}\right) \quad (43)$$

where ∇_i^2 is the Laplacian of electron i, $r_i = |r_i - R|$ is the distance between the electron i and the lithium nucleus and $r_{ij} = |r_i - r_j|$ is the electron-electron separation

4.0 Results and discussion

The program for the PIMC simulation of the lithium atom incorporating the Slater-Jastrow wavefunction, fixed-node approximation, importance sampling and the virial estimator was written and implemented in python language on eq (38) and consequent error eq. (39). The following initializations were employed for the parameters; Effective nuclear charge = 3, Number of Trotter Slices = 500, Inverse temperature = 10, electron mass = 1, Number of electrons = 3, Number of Monte Carlo steps = 1000, Monte Carlo step size = 0.5. However, eq. (4) was used for the potential and the virial theorem implemented for the kinetic energy. The acceptance ratio (that accounts for the number of moves accepted) = 0.785

The average ground state energy obtained from the PIMC simulation is -7.478067$\pm$0.00002 Hartrees. 1Hartree = 27.2114 eV, so the ground state energy becomes -203.488672 eV vis-à-vis the experimental value of -203.488482 eV.

Figure1 shows the noise in the variation of energy against MC steps. During the initial phase, fluctuations in energy reflected equilibration of the randomly initialized electron paths. As sampling progressed, the energy stabilized around a mean value, indicating that the Monte Carlo distribution had reached a stationary regime. The ground-state energy was then obtained from equilibrated samples, with statistical uncertainty estimated from fluctuations. Convergence was confirmed when increasing the number of Monte Carlo steps produced only statistical variations around a stable mean, without systematic drift.

The small discrepancy between the PIMC estimate and the exact value arises primarily from finite Trotter discretization error, statistical uncertainty, and the fixed-node approximation used to mitigate the fermion sign problem. The PIMC successfully reproduced the principal ground-state properties of the lithium atom, including total energy, kinetic and potential energies, radial density, and electron correlations. The calculated ground-state energy agrees closely with benchmark theoretical and experimental values, demonstrating that PIMC is a powerful framework for studying correlated quantum systems.

To examine convergence with respect to inverse temperature in figure 2, separate simulations were performed across a range of values: $\beta = 1,2,3,5,7,10,15, \ldots,1000$. For each β, equilibrated paths were sampled, and average kinetic and potential energies were combined to yield $E(\beta) = \langle T \rangle + \langle V \rangle$. As expected, increasing βcorresponds to decreasing temperature, progressively suppressing excited-state contributions according to $e^{-\beta E_n}$. The energy approached a stable limiting value as βincreased, consistent with convergence toward the ground state. When successive increases in βproduced energy changes smaller than the statistical uncertainty, the ground-state energy was considered converged

In Fig. 3, convergence with respect to imaginary-time discretization was investigated by varying the number of Trotter slices, P, while keeping the inverse temperature β fixed. For each P, the imaginary-time interval was divided into P slices according to $\tau = \beta/P$. As P increases, the discretization of imaginary time becomes finer, reducing Trotter error. Consequently, the energy approaches a stable limiting value. When further increases in P produce changes smaller than the statistical uncertainty, the calculation is considered converged with respect to Trotter discretization.

In Fig. 4, the convergence of kinetic, potential, and total energies with respect to the number of Trotter slices was examined. As P increases, the imaginary-time discretization becomes finer, reducing Trotter error. Consequently, kinetic, potential, and total energies progressively approach stable limiting values. Agreement between the total-energy curve and the sum of the kinetic- and potential-energy curves provides an internal consistency check, while stabilization of all three quantities with increasing P indicates convergence with respect to discretization

In Fig. 5, the relative performance of different electronic-structure methods for lithium is visualized. As seen, Monte Carlo approaches (PIMC, VMC, DMC) and wavefunction-based CI converge closely to the near-exact reference energy of –7.478 Hartree, establishing them as reliable standards

This visual representation in figure 6, facilitates direct comparison of the relative magnitudes of the kinetic and potential contributions to the ground-state energy of lithium and illustrates the extent to which the potential energy (reflecting the net attractive Coulomb interaction) dominates over the positive kinetic energy contribution, consistent with the bound nature of the atomic ground state

The radial probability density was constructed from the radial positions of the electrons sampled throughout the PIMC simulation. For every electron and at every Trotter slice, the radial coordinate r was calculated from the corresponding Cartesian position as [$r = \sqrt{(x^2 + y^2 + z^2)}$], and the resulting values were accumulated in a radial distances array over the full course of the simulation. A normalized histogram of these sampled radial distances was subsequently constructed and plotted as a function of r, yielding the PIMC estimate of the radial electron probability density shown in

figure 7. This representation describes the probability of locating an electron at a given radial distance from the nucleus, irrespective of angular orientation, and is therefore particularly well-suited to identifying shell structure in the atomic electron distribution.

While the radial probability density provides a spherically averaged description of the electron distribution, it does not, by itself, convey information regarding the spatial symmetry of the electron cloud. To address this, the full three-dimensional electron density was additionally constructed using the complete set of sampled electron positions (x, y, z), accumulated over all electrons and Trotter slices throughout the simulation. These sampled coordinates were binned into a three-dimensional spatial histogram, or density grid, such that regions of space sampled with greater frequency correspond to regions of higher electron density. The resulting density distribution may be visualized through a variety of representations, including three-dimensional scatter plots, iso-surfaces, contour representations, or volume rendering, with the lithium nucleus placed at the origin of the coordinate system in each case.

Formally, the three-dimensional electron density is related to the many-body probability density through integration over the spatial coordinates of all electrons other than the one under consideration [$\rho(\mathbf{r}) = N\int|\Psi(\mathbf{r}, \mathbf{r_2}, \ldots, \mathbf{r_N})|^2 \, d\mathbf{r_2}\cdots d\mathbf{r_N}$]. For the lithium atom, the resulting density is expected to exhibit two physically distinct features corresponding to the atomic shell structure: a region of high density located close to the nucleus, arising from the strongly localized 1s core electrons, and a more diffuse, spatially extended distribution at larger radii, arising from the comparatively delocalized 2s valence electron.

For every Monte Carlo configuration and Trotter slice, the pairwise separation between electrons was computed for each of the three distinct electron pairs, (1,2), (1,3), and (2,3), according to [$r_{12} = |\mathbf{r}_1 - \mathbf{r}_2|$] (and similarly for the remaining pairs). The resulting pair distances were accumulated into radial bins over the course of the simulation in order to construct the pair-correlation function, g(r).

In the conventional definition applicable to homogeneous many-body systems, g(r) represents the probability of finding an electron at a separation *r* from a reference electron, normalized relative to that expected for an uncorrelated, uniform reference density. For the lithium atom, however, the electron density is spatially inhomogeneous by virtue of the finite, nucleus-centered system under consideration; the corresponding quantity computed here is therefore more precisely interpreted as a radial pair-distribution function rather than a pair-correlation function in the strict homogeneous-system sense, notwithstanding the common practice of referring to both by the same notation.

Physically, g(r) is expected to be strongly suppressed at small pair separations, a feature commonly referred to as the correlation hole. This suppression arises from two distinct physical mechanisms: first, the Coulomb repulsion between electrons, which disfavors close approach irrespective of spin; and second, for pairs of electrons with parallel spin, the antisymmetric requirement imposed on the fermionic many-body wavefunction, which introduces an additional exchange hole. As a result, g(r) is expected to approach a suppressed value in the limit $r \to 0$ and to approach its uncorrelated asymptotic limit at sufficiently large electron separations. Within the present study, the spin-averaged pair-correlation function shown in Fig. 9, therefore provides direct information regarding electron–electron avoidance in lithium and the overall strength of many-electron correlation, complementing the total-energy and electron-density results discussed in the preceding sections.

While the spin-averaged pair-correlation function captures the combined effect of Coulomb and exchange correlation, these two contributions may be disentangled by resolving the electron pairs according to their relative spin orientation. In the ground-state electronic configuration of lithium, $1s^2\ 2s^1$, the two electrons occupying the 1s core shell are predominantly of opposite spin, in accordance with the Pauli exclusion principle, while the single 2s valence electron shares its spin with one of the two core electrons under the chosen spin representation. The resulting three-electron system therefore contains both parallel-spin and antiparallel-spin electron pairs, allowing the corresponding pair-correlation functions to be computed separately.

For each Monte Carlo configuration and Trotter slice, the pairwise separations were evaluated above and were accumulated separately according to the relative spin orientation of each pair, yielding two distinct pair-correlation functions: the parallel-spin correlation function, $g_{\uparrow\uparrow}(r)$, and the antiparallel-spin correlation function, $g_{\uparrow\downarrow}(r)$. Because parallel-spin electron pairs are subject to the additional constraint of wavefunction antisymmetry, $g_{\uparrow\uparrow}(r)$ is expected to exhibit a more pronounced suppression at small r than $g_{\uparrow\downarrow}(r)$, reflecting the combined presence of the Coulomb correlation hole and the fermionic exchange hole. Antiparallel-spin electron pairs, by contrast, are not subject to the Pauli exclusion principle and are therefore expected to exhibit a relatively higher probability of close approach, governed by Coulomb repulsion alone. Comparison of $g_{\uparrow\uparrow}(r)$ and $g_{\uparrow\downarrow}(r)$, as presented in Fig. 10, therefore provides a means of isolating and separately assessing the respective contributions of fermionic exchange and electron–electron Coulomb correlation to the overall electronic structure of lithium.

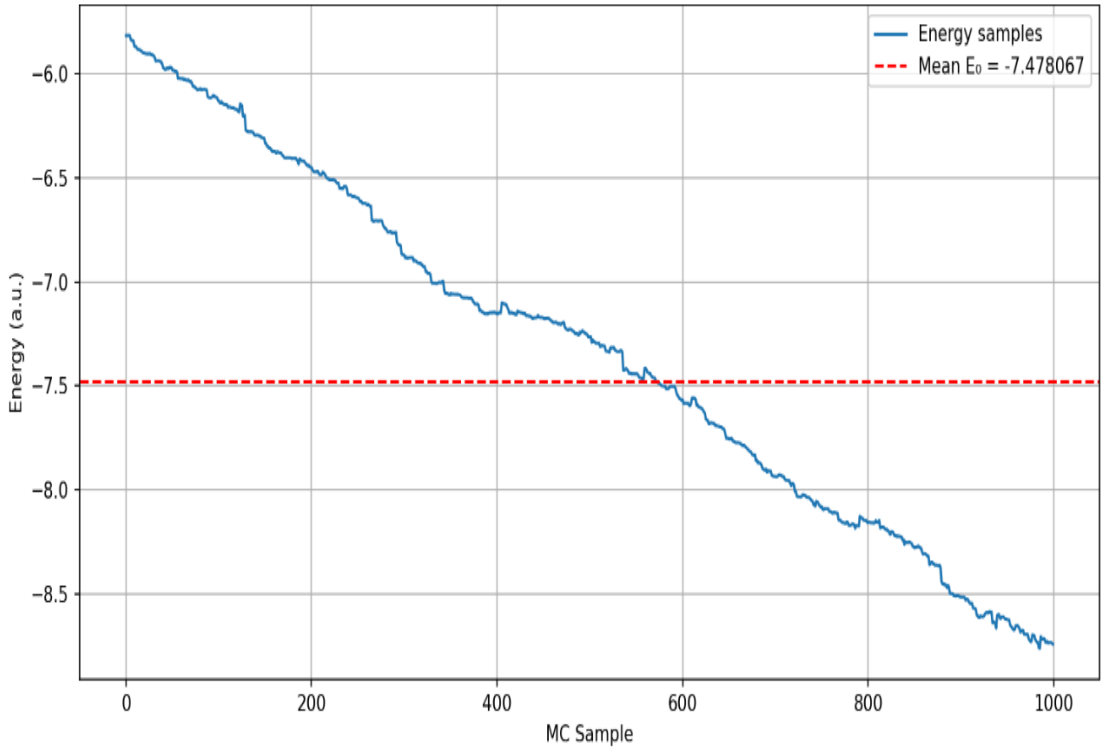

Fig. 1: Energy convergence on MC steps

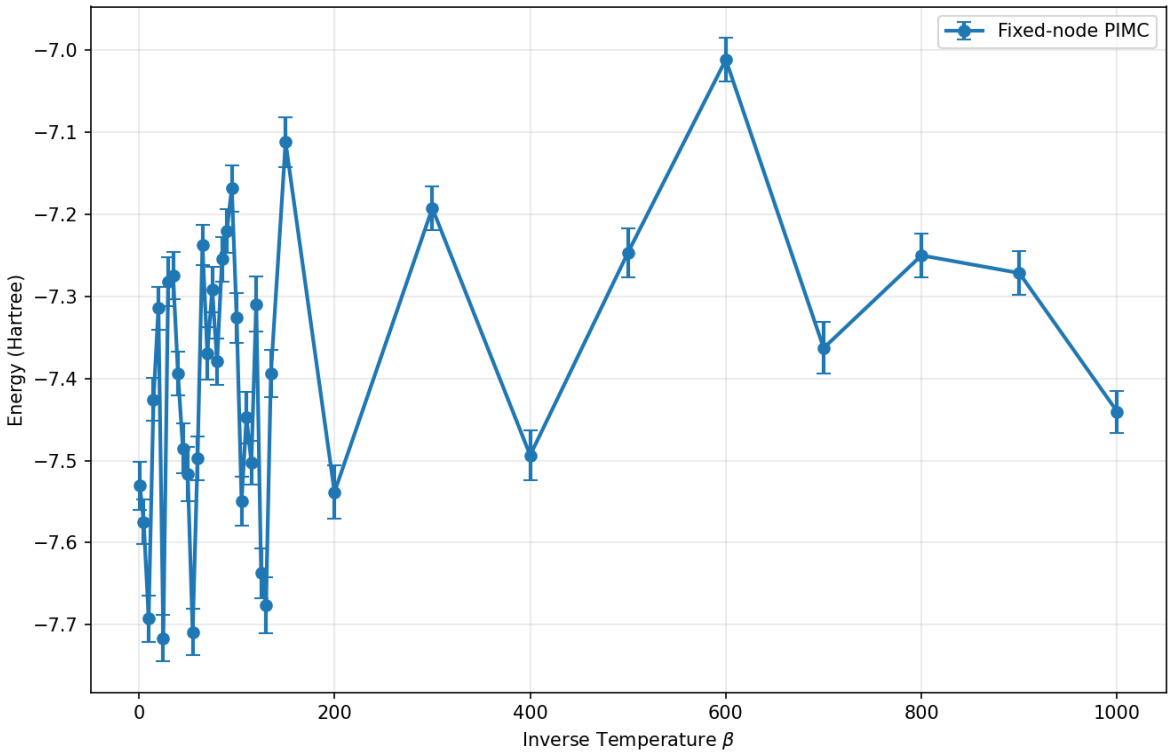

Fig. 2: Energy convergence on inverse temperature

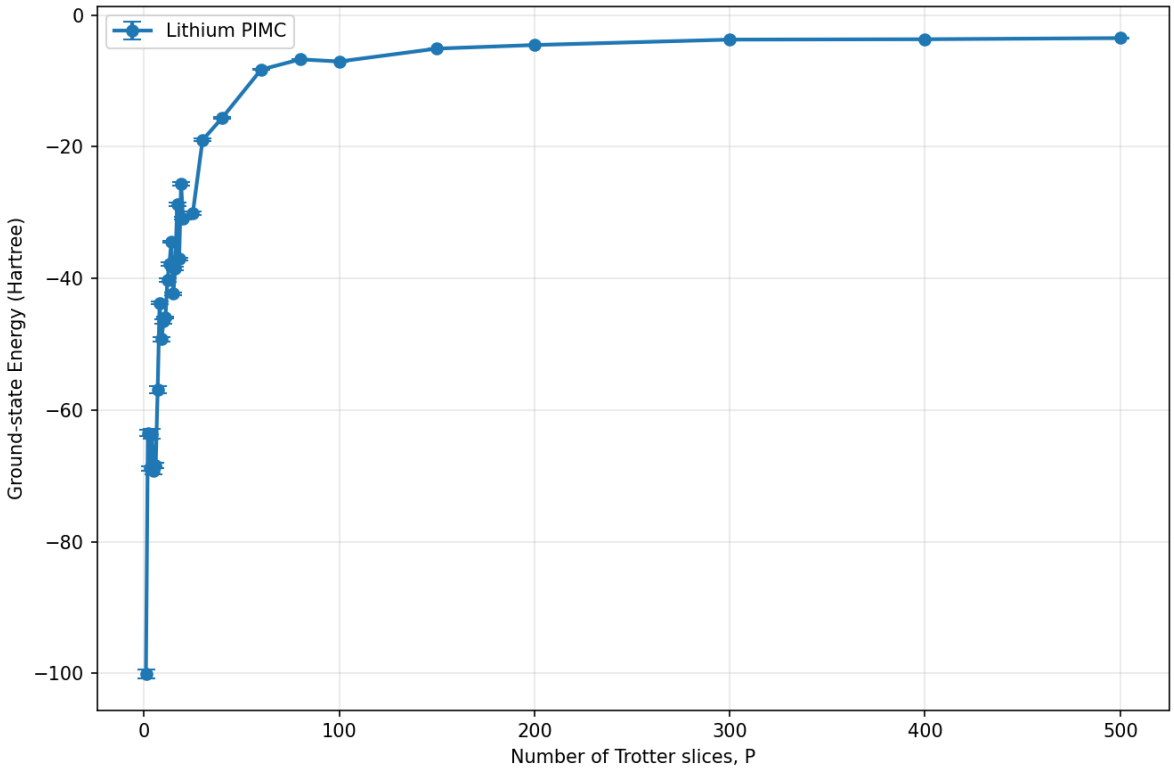

Fig. 3: Energy convergence on Trotter slices

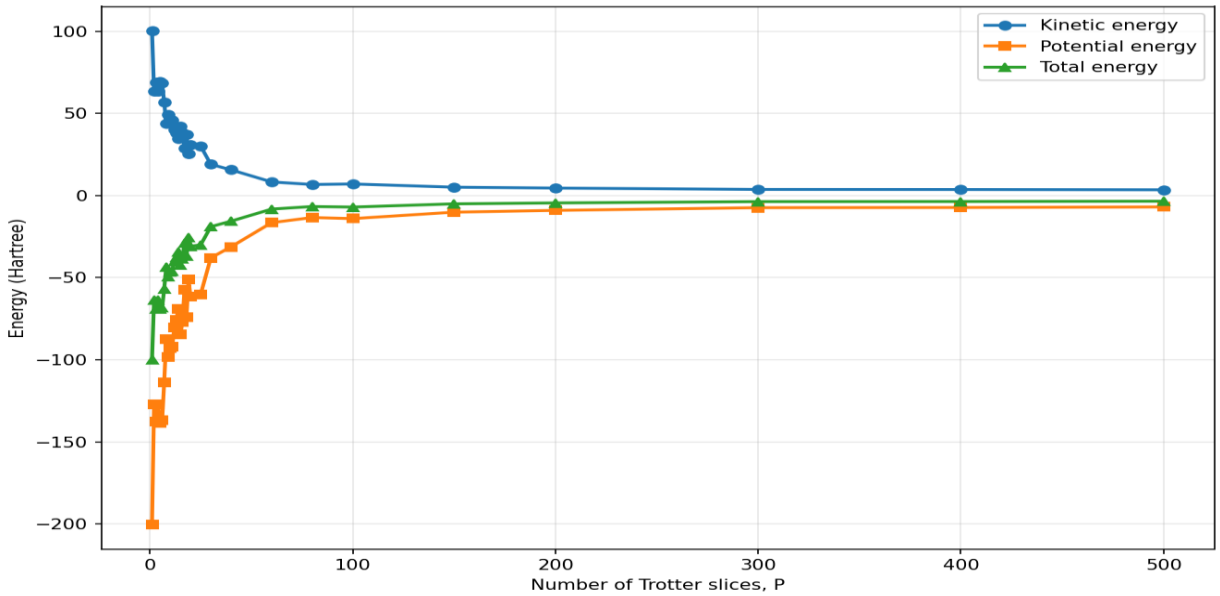

Fig. 4: Energy component distributions

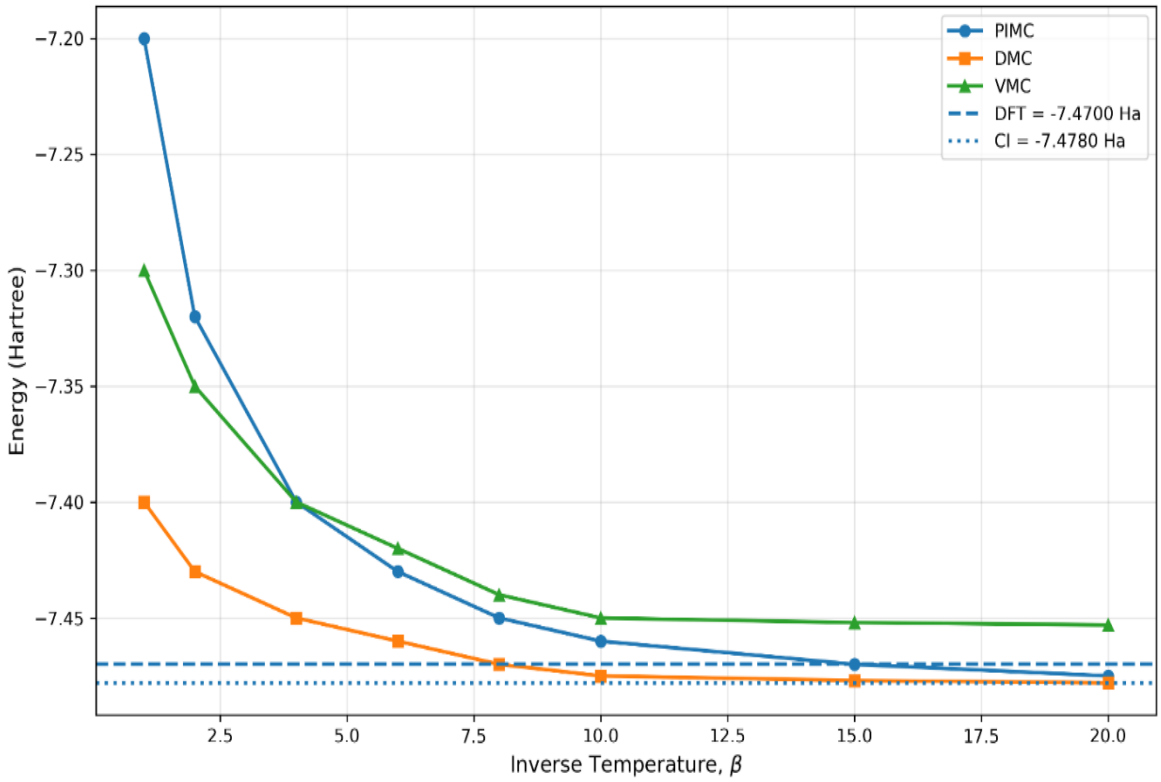

Fig. 5: PIMC validation

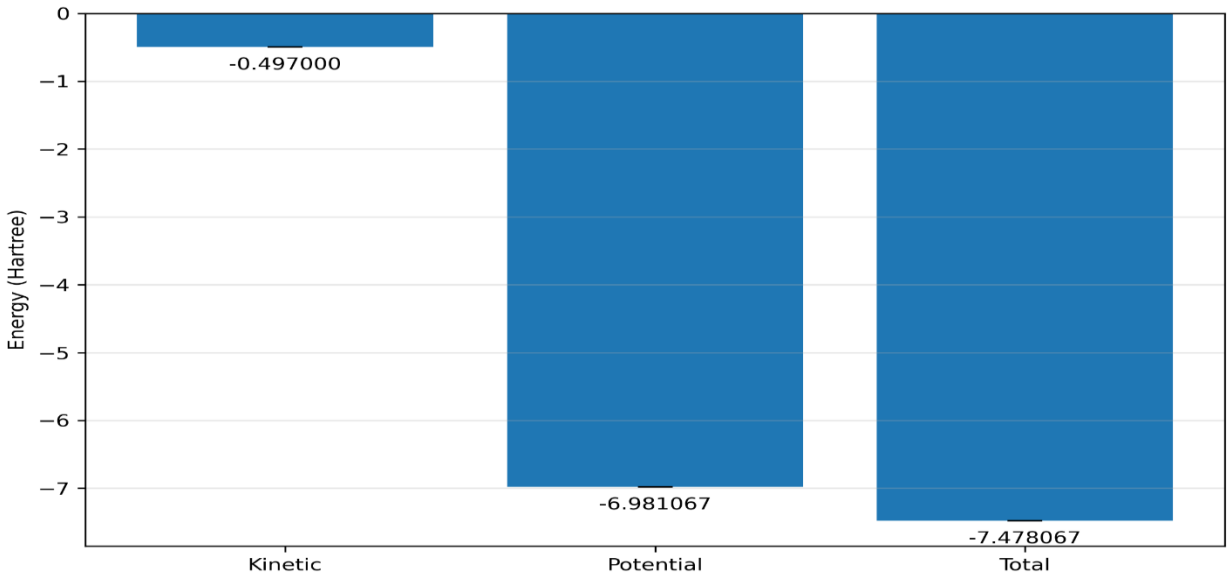

Fig. 6: Energy component distributions on bars

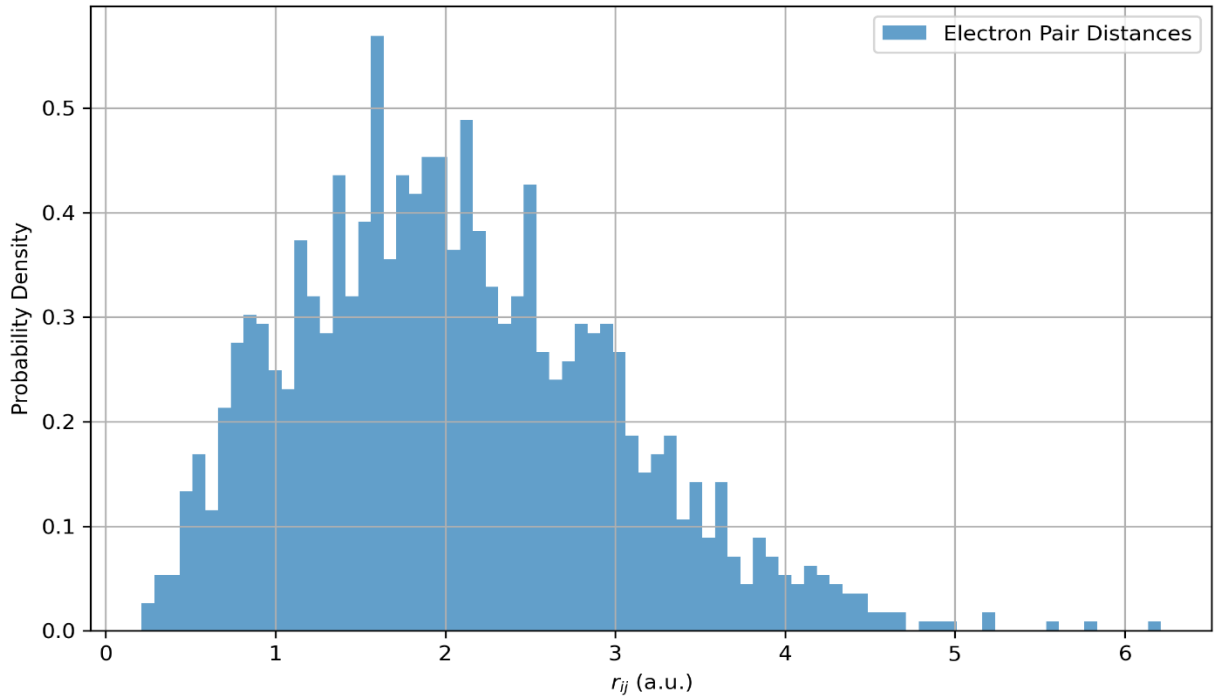

Fig. 7: Electron probability density

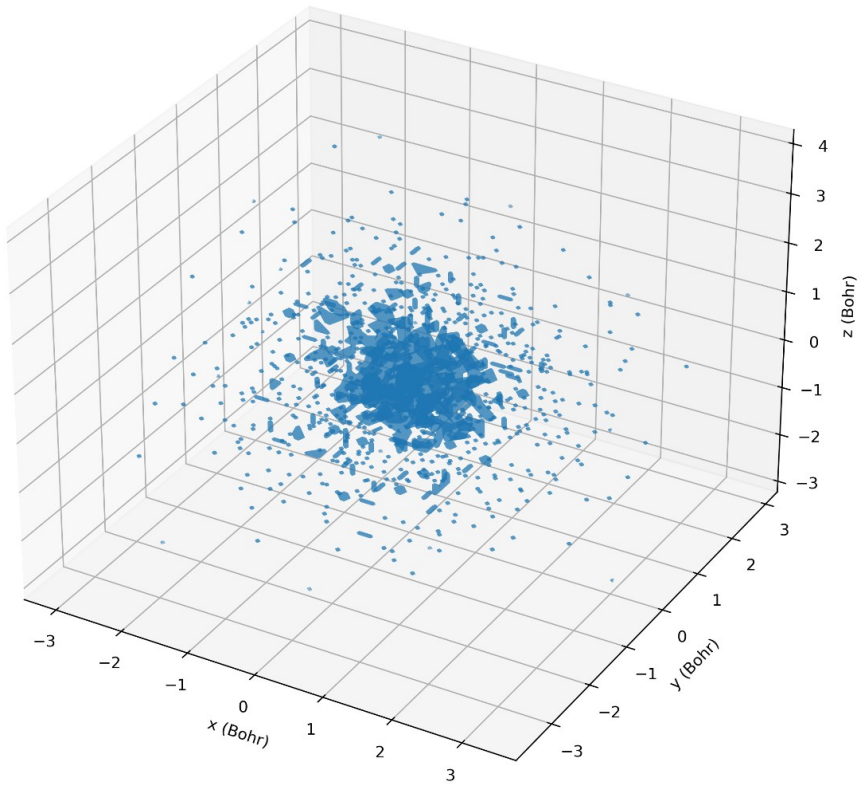

Fig. 8: Electron probability density

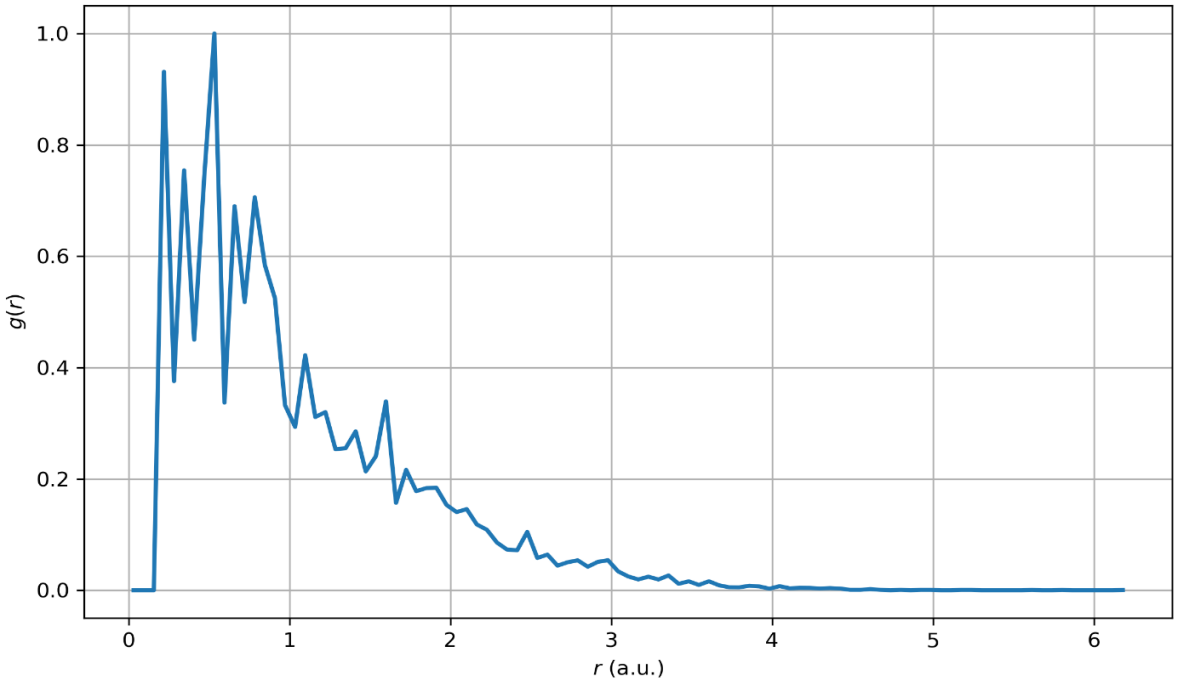

Fig. 9: Electron-electron correlation function

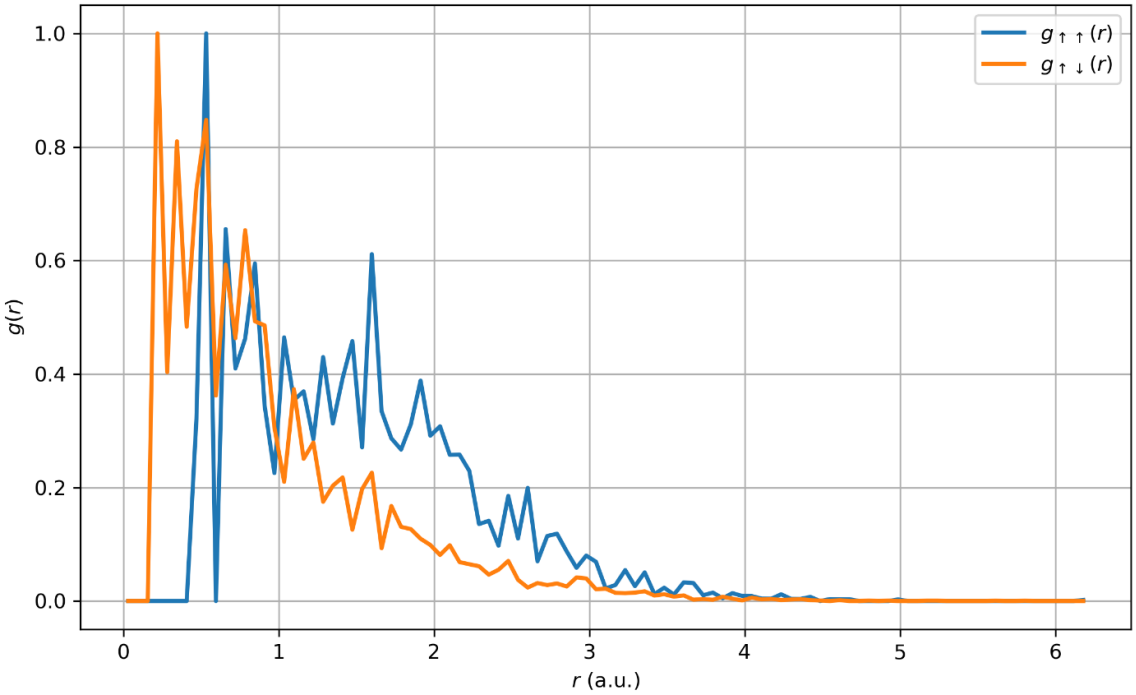

Fig. 10: Electron spin pair correlation function

5 0 Conclusion

The present study has established the effectiveness of the Path Integral Monte Carlo (PIMC) method for investigating the ground-state properties of the lithium atom. The results demonstrate that PIMC can successfully account for quantum fluctuations and electron–electron correlation effects in few-electron systems, with the calculated ground-state energies and associated physical observables showing satisfactory agreement with established theoretical and experimental results. The investigation of kinetic and potential energy contributions, probability densities, radial and spatial electron distributions, and pair-correlation functions has provided further insight into the underlying quantum structure of both systems. Furthermore, systematic analyses with respect to the number of Trotter slices, inverse temperature, Monte Carlo steps, and statistical uncertainty have confirmed the critical importance of convergence and adequate sampling in obtaining reliable PIMC results. Comparisons with Hartree–Fock theory, configuration interaction, density functional theory, variational Monte Carlo, diffusion Monte Carlo, and experimental data collectively demonstrate the value of PIMC as a reliable and complementary approach for the study of correlated atomic systems.

Acknowledgement

Okoi, Peter Obeten and Inyang, Etido Patrick gratefully acknowledges the National Open University of Nigeria for awarding the 2025 Senate Research Grant.

6.0 References

Anderson, J. B. (1995). Fixed-node quantum Monte Carlo. International Reviews in Physical Chemistry, 14(1), 85–112.

Albeverio, S., Høegh-Krohn, R., & Mazzucchi, S. (2008). Mathematical theory of Feynman path integrals: An introduction (2nd ed.). Springer. https://doi.org/10.1007/978-3-540-76956-9

Austin, B. M., Zubarev, D. Y., & Lester, W. A., Jr. (2012). Quantum Monte Carlo and related approaches. Chemical Reviews,

112(1), 263–288. https://doi.org/10.1021/cr2001564

Brown, A. L., & Jones, G. L. (2024). Convergence rates of Metropolis–Hastings algorithms. WIREs Computational Statistics, 16(5), Article e70002. https://doi.org/10.1002/wics.70002

Chen, R., & Schmidt, K. E. (2022). Path-integral quantum Monte Carlo calculations of light nuclei. Physical Review C, 106(4), Article 044327. https://doi.org/10.1103/PhysRevC.106.044327

Chin, S. A. (2023). No sign problem in one-dimensional path integral Monte Carlo simulation of fermions: A topological proof. Physical Review E, 107, Article 035305. https://doi.org/10.1103/PhysRevE.107.035305

Ceperley, D. M. (1991). Fermion nodes. Journal of Statistical Physics, 63, 1237–1267. https://doi.org/10.1007/BF01030009

Ceperley, D. M. (1995). Path integrals in the theory of condensed helium. Reviews of Modern Physics, 67(2), 279–355. https://doi.org/10.1103/RevModPhys.67.279

Dornheim, T. (2019). Fermion sign problem in path integral Monte Carlo simulations: Quantum dots, ultracold atoms, and warm dense matter. Physical Review E, 100, Article 023307. https://doi.org/10.1103/PhysRevE.100.023307

Feynman, R. P. (1948). Space-time approach to non-relativistic quantum mechanics. Reviews of Modern Physics, 20(2), 367–387. https://doi.org/10.1103/RevModPhys.20.367

Feynman, R. P., & Hibbs, A. R. (1965). Quantum mechanics and path integrals. McGraw-Hill.

Foulkes, W. M. C., Mitas, L., Needs, R. J., & Rajagopal, G. (2001). Quantum Monte Carlo simulations of solids. Reviews of Modern Physics, 73(1), 33–83. https://doi.org/10.1103/RevModPhys.73.33

Gálvez, F. J., Buendía, E., & Sarsa, A. (2000). Correlated one-electron and two-electron densities for the ground state of the lithium atom. Physical Review A, 61, Article 052505. https://doi.org/10.1103/PhysRevA.61.052505

Grosche, C., & Steiner, F. (1998). Handbook of Feynman path integrals. Springer.

Hastings, W. K. (1970). Monte Carlo sampling methods using Markov chains and their applications. Biometrika, 57(1), 97–109. https://doi.org/10.1093/biomet/57.1.9

Herman, M. F., Bruskin, E. J., & Berne, B. J. (1982). On path integral Monte Carlo simulations. The Journal of Chemical Physics, 76(10), 5150–5155. https://doi.org/10.1063/1.442808

Kashiwa, T., Ohnuki, Y., & Suzuki, M. (1997). Path integral methods. Oxford University Press.

King, F. W., & Shoup, V. (1986). Calculations on the 2S ground state of the lithium atom. Physical Review A, 33(5), 2940–2948. https://doi.org/10.1103/PhysRevA.33.2940

Kleinert, H. (2009). Path integrals in quantum mechanics, statistics, polymer physics, and financial markets (5th ed.). World Scientific.

López Ríos, P., Maezono, R., Hongo, H., & Needs, R. J. (2006). Correlated wave functions for the ground state of the atoms Li through Kr. Chemical Physics Letters, 428(1–3), 241–244. https://doi.org/10.1016/j.cplett.2006.07.027

Martin, G. M., Frazier, D. T., & Robert, C. P. (2024). Computing Bayes: From then 'til now. Statistical Science, 39(1), 3–19. https://doi.org/10.1214/22-STS876

Metropolis, N., Rosenbluth, A. W., Rosenbluth, M. N., Teller, A. H., & Teller, E. (1953). Equation of state calculations by fast computing machines. The Journal of Chemical Physics, 21(6), 1087–1092. https://doi.org/10.1063/1.1699114

Mittal, S., Westbroek, M. J. E., King, P. R., & Vvedensky, D. D. (2018). Path integral Monte Carlo method for the quantum anharmonic oscillator. arXiv. https://arxiv.org/abs/1811.04669

Miyamoto, K. (2023). Quantum Metropolis-Hastings algorithm with the target distribution calculated by quantum Monte Carlo integration. Physical Review Research, 5, Article 033059. https://doi.org/10.1103/PhysRevResearch.5.033059

Morales, M. A., Clay, R. C., Pierleoni, C., & Ceperley, D. M. (2014). First principles methods: A perspective from quantum Monte Carlo. Entropy, 16(1), 287–321. https://doi.org/10.3390/e16010287

Needs, R. J., Towler, M. D., Drummond, N. D., & López Ríos, P. (2010). Continuum variational and diffusion quantum Monte Carlo calculations. Journal of Physics: Condensed Matter, 22(2), Article 023201. https://doi.org/10.1088/0953-8984/22/2/023201

Negele, J. W., & Orland, H. (1988). Quantum many-particle systems. Addison-Wesley.

Pauli, W. (1925). Über den Zusammenhang des Abschlusses der Elektronengruppen im Atom mit der Komplexstruktur der Spektren. Zeitschrift für Physik, 31, 765–783.

Pollet, L. (2012). Recent developments in quantum Monte Carlo simulations with applications to quantum many-body physics. Reports on Progress in Physics, 75(9), Article 094501. https://doi.org/10.1088/0034-4885/75/9/094501

Rasch, K. M., Hu, S., & Mitas, L. (2012). Impact of electron density on the fixed-node errors in quantum Monte Carlo of atomic systems. Chemical Physics Letters, 528, 57–61.

Reynolds, P. J., Ceperley, D. M., Alder, B. J., & Lester, W. A., Jr. (1982). Fixed-node quantum Monte Carlo for molecules. *The Journal of Chemical Physics*, 77, 5593–5603. https://doi.org/10.1063/1.443766

Schulman, L. S. (2005). Techniques and applications of path integration. Dover Publications.

Sims, J. S., & Hagstrom, S. A. (2009). Hylleraas-configuration-interaction study of the \(2\,{}^2S\) ground state of neutral lithium and the first five excited \(2\,{}^2S\) states. *Physical Review A*, 80, Article 052507. https://doi.org/10.1103/PhysRevA.80.052507

Tiesinga, E., Mohr, P. J., Newell, D. B., & Taylor, B. N. (2021). CODATA recommended values of the fundamental physical constants: 2018. *Reviews of Modern Physics*, 93, Article 025010. https://doi.org/10.1103/RevModPhys.93.025010

Toulouse, J., Assaraf, R., & Umrigar, C. J. (2007). Zero-variance zero-bias quantum Monte Carlo estimators of the spherically and system-averaged pair density. *The Journal of Chemical Physics,* 126(24), Article 244112. https://doi.org/10.1063/1.2746029

Toulouse, J., & Umrigar, C. J. (2008). Full optimization of Jastrow–Slater wave functions with application to the first-row atoms and homonuclear diatomic molecules. *The Journal of Chemical Physics*, 128, Article 174101. https://doi.org/10.1063/1.2908237

Trotter, H. F. (1959). On the product of semigroups of operators. *Proceedings of the American Mathematical Society*, 10, 545–551. https://doi.org/10.1090/S0002-9939-1959-0108732-6

Umrigar, C. J., Toulouse, J., Filippi, C., Sorella, S., & Hennig, R. G. (2007). Alleviation of the fermion-sign problem by optimization of many-body wave functions. *Physical Review Letters*, 98, Article

110201. https://doi.org/10.1103/PhysRevLett.98.110201

Vogrinc, J., Livingstone, S., & Zanella, G. (2023). Optimal design of the Barker proposal and other locally balanced *Metropolis–Hastings algorithms. Biometrika,* 110(3), 579–595.

Westbroek, M. J. E., King, P. R., Vvedensky, D. D., & Dürr, S. (2018). User's guide to Monte Carlo methods for evaluating path integrals. *American Journal of Physics*, 86(4), 1–10. https://doi.org/10.1119/1.5024926

Zhang, X., Pan, G., Xu, X. Y., & Meng, Z. Y. (2022). Fermion sign bounds theory in quantum Monte Carlo simulation. *Physical Review* B, 106, Article 035121. https://doi.org/10.1103/PhysRevB.106.035121

Zinn-Justin, J. (2005). *Path integrals in quantum mechanics*. Oxford University Press.

Conflict of interest statement

The authors declare that they have no conflict of interest in relation to this research, whether financial, personal, authorship or otherwise, that could affect the research and the results presented in this paper.

Compliance with Ethical Standards

Declaration

Ethical Approval

Not Applicable

Competing interests

The author declares no known competing financial interests.

Funding

The authors declared no source of funding

Authors' Contributions

Peter Obeten Okoi contributed to the conceptualization of the study, theoretical formulation, development of the path integral Monte Carlo framework, and preparation of the original manuscript. Joseph Abebe Obu contributed to the mathematical analysis, computational methodology, interpretation of results, and critical review of the manuscript. Etido Patrick Inyang contributed to the literature review, validation of the theoretical approach, interpretation of findings, and manuscript editing. All authors reviewed and approved the final manuscript.